Computers in Biology and Medicine 153 (2023) 106458

Contents lists available at ScienceDirect

Computers in Biology and Medicine

journal homepage: www.elsevier.com/locate/compbiomed

Computational modeling of multiple myeloma interactions with resident bone marrow cells

Pau Urdeitx [a,b,c], S. Jamaleddin Mousavi [d], Stephane Avril [d,e], Mohamed H. Doweidar [a,b,c,*]

[a] School of Engineering and Architecture (EINA), University of Zaragoza, Zaragoza, 50018, Spain
[b] Aragon Institute of Engineering Research (I3A), University of Zaragoza, Zaragoza, 50018, Spain
[c] Biomedical Research Networking Center in Bioengineering, Biomaterials and Nanomedicine (CIBER-BBN), Zaragoza, 50018, Spain
[d] Mines Saint-Étienne, University of Lyon, University of Jean Monnet, INSERM, Saint-Etienne, 42023, France
[e] Institute for Mechanics of Materials and Structures, TU Wien-Vienna University of Technology, Vienna, 1040, Austria

ARTICLE INFO

Keywords:
In-silico model
Computational cell mechanics
Finite element method
Cell Mechanobiology
Multiple myeloma cells

ABSTRACT

The interaction of multiple myeloma with bone marrow resident cells plays a key role in tumor progression and the development of drug resistance. The tumor cell response involves contact-mediated and paracrine interactions. The heterogeneity of myeloma cells and bone marrow cells makes it difficult to reproduce this environment in *in-vitro* experiments. The use of *in-silico* established tools can help to understand these complex problems.

In this article, we present a computational model based on the finite element method to define the interactions of multiple myeloma cells with resident bone marrow cells. This model includes cell migration, which is controlled by stress–strain equilibrium, and cell processes such as proliferation, differentiation, and apoptosis.

A series of computational experiments were performed to validate the proposed model. Cell proliferation by the growth factor IGF-1 is studied for different concentrations ranging from 0–10 ng/mL.

Cell motility is studied for different concentrations of VEGF and fibronectin in the range of 0–100 ng/mL. Finally, cells were simulated under a combination of IGF-1 and VEGF stimuli whose concentrations are considered to be dependent on the cancer-associated fibroblasts in the extracellular matrix.

Results show a good agreement with previous *in-vitro* results. Multiple myeloma growth and migration are shown to correlate linearly to the IGF-1 stimuli. These stimuli are coupled with the mechanical environment, which also improves cell growth. Moreover, cell migration depends on the fiber and VEGF concentration in the extracellular matrix. Finally, our computational model shows myeloma cells trigger mesenchymal stem cells to differentiate into cancer-associated fibroblasts, in a dose-dependent manner.

1. Introduction

Multiple myeloma develops from malignant plasma cells, which invade bone marrow (BM) [1]. Its heterogeneity and complex interactions with BM resident cells make it difficult to develop effective strategies for cancer treatments [2,3]. Despite the advances in diagnosis and novel pharmacological therapies, to this day, it remains incurable and represents the second most common hematological malignancy [4,5]. Multiple myeloma cells (MMCs) interactions with BM resident cells, such as mesenchymal stem cells (MSCs), macrophages, and osteoblasts, play a key role in the therapies' effectiveness and tumor progression. For instance, interactions of MMCs with osteoblasts reduced the levels of osteoprotegerin, which may lead to an increase in osteoclasts differentiation. Consequently, an increase in bone resorption and a reduction in net bone mass can be observed, with osteoporosis being a frequently observed disorder in patients with multiple myeloma [6]. For its part, interactions with MSCs play a key role in tumor progression and drug resistance development [7,8]. This MMCs response, due to the interaction with MSCs, is associated with both contact-mediated and paracrine signaling. The MMC–MSC interaction results in the secretion of different cytokines, and growth factors, which promote MMCs proliferation, enhance cell migration, inhibit cell apoptosis and confer drug resistance [3].

Among these factors, MSCs secrete Vascular Endothelial Growth Factor (VEGF), which has been reported to enhance MMCs growth,

* Corresponding author at: School of Engineering and Architecture (EINA), University of Zaragoza, Zaragoza, 50018, Spain.
E-mail address: mohamed@unizar.es (M.H. Doweidar).

https://doi.org/10.1016/j.compbiomed.2022.106458
Received 24 October 2022; Received in revised form 8 December 2022; Accepted 19 December 2022
Available online 26 December 2022

migration, and angiogenesis [7]. K. Lambert et al. observed that the Transforming Growth Factor-β (TGF-β) receptor, which is usually down-regulated in MMCs, is directly associated with the VEGF response. Thus, restoring the expression of this receptor could inhibit the cell response to the VEGF in terms of cell growth, proliferation, and motility [9]. For its part, Interleukin 6 (IL-6), a cytokine expressed by different cells in the BM such as T cells, B cells, monocytes, and MSCs, increases cell growth and inhibits cell apoptosis [8,10,11]. Through the cell–cell contact with the MSCs, IL-6 confers contact-mediated drug resistance to the MMCs [7,8]. Other factors, such as Insulin-like Growth Factor 1 (IGF-1), Interleukin-1 (IL-1), Hepatocyte Growth Factor (HGF), TGF-β, and Stromal cell-Derived Factor-1α (SDF-1α), are reported to play an important role in MMCs growth, proliferation, and migration [6,12,13].

Besides, it has been reported that the advantages conferred by MSCs are highly relevant for homing and tumor growth, where MMCs play an active role in the recruitment of MSCs, generating alterations in MSCs, thereby increasing their pro-tumor effect [7,11]. Thus, in the study presented by Y. Feng et al. they observed how the cells of patients affected by multiple myeloma presented significant changes in their gene expression profiles and mechanical properties [10]. This was also corroborated by D. Wu et al. who cocultured MSCs with MMCs, and observed an increase in the MSCs stiffness and Focal Adhesion Kinase (FAK) activation [11]. They also observed that MSCs revert MMCs to a less differentiated phenotype through IL-6 and adhesive interactions, thus concluding that cell adhesions were crucial in the development of drug resistance [11]. These phenotype changes, reported by these and other authors, suggest the MSCs, among other cell types, as a possible origin of Cancer-Associated Fibroblasts (CAFs) cell phenotype [8,14]. The complex interactions between cells, with multiple factors acting simultaneously, as well as the heterogeneity of the cell populations of MMCs and CAFs, make it difficult to understand the tumor niche and reproduce in *in-vitro* experiments to study MMCs drug response [15,16]. In this sense, computational models, capable of considering these effects, individually and coupled, allow us to provide new perspectives in the study of the growth of malignant MMCs.

Computational models are classified into two main groups: continuous models and discrete models. Continuous models, based on partial and ordinary differential equations, describe the dynamics of big cell populations as well as the diffusion of species [17]. Although they have been shown to be effective in the study of wound healing [18], bone remodeling [19], nutrient consumption for bioreactors design [20,21], and scaffolds design [22–24], these models do not recognize the individualized cell response, or the effects due to cell–cell contacts and adhesion, which play a key role in tumor's growth and drug resistance development [11]. For their part, discrete models focus their study on the specific conditions of each individualized cell, being capable of reproducing cell–cell adhesions and the response they trigger [25–27]. In fact, different models are applied to the study of cell differentiation [28,29], proliferation [30–32], cell morphology [33–36], migration [25,37–39], angiogenesis [27] and cell-level tissue architectures [30,31]. However, to the authors' knowledge, in the literature, there is no model where complex interactions of MMCs with resident BM cells in 3D environments, including cell–cell contacts, enhancement of mechanical properties, and the cell growth response. Thus, here we present an *in-silico* agent-based model, where MMCs interactions with BM resident cells and the cells' response, are studied. This model includes cell growth and migration enhancement due to the effect of IGF-1, and VEGF stimulation, and differentiation of MSC into CAF due to the TGF-β stimulation. These effects are coupled with direct cell–cell interactions and the Extracellular matrix (ECM) stiffness.

2. Methods

The spread of cancer cells from the primary tumor, as well as the formation of stable cell aggregates, depends, among others, on the ability of cells to mechanically interact with their environment and with other neighboring cells [40,41]. In fact, cell migration is a cellular process where the main internal components of the cell intervene in a series of coordinated events that culminate in cell translocation [42,43]. Cells interact with their environment by deforming the ECM through focal adhesions. ECM stiffness, among other factors, determines cell polarization and thus the direction of the cell migration process. Therefore, it is possible to define cell motility as an equilibrium between the active forces of the cell and the cell–ECM deformations [30].

2.1. Modeling of cell migration

Our cell mechanical model assumes that cell internal deformations are a result of cell–cell and cell–ECM interactions [26]. The actin–myosin (AM) bundles, which are considered as a part of the cytoskeleton (CSK), are the main components that actively develop contractile forces within the cell, whereas other components of the CSK along with the cell membrane, act as resistive elements that oppose the cell internal deformation. The mechanical model of the cell differentiates the active and passive cell components from their mechanical contribution perspective. Hence, cell internal deformations are defined through the stress–strain equilibrium between the cell internal components and the ECM, which includes the equilibrium between the AM contraction and the whole cell resistance to the deformation. Thus, the cell internal deformations generate cell internal stresses that are transmitted to the ECM through the CSK and the focal adhesions. The cell traction forces, which are dependent on the cell's internal stresses, are defined as [28,30]:

$$\mathbf{F}_{trac} = \sum_{i=1}^{n} \sigma_i \; S \; \kappa \; n_r \; \psi \; \mathbf{e}_i, \tag{1}$$

where κ, n_r, and ψ are the binding constant, the number of available receptors in the cells, and the Fibronectin (FN) concentration, respectively, which denotes the strength of the cell–ECM adhesion. σ_i are the cell internal stresses at each membrane node on the cell surface, located at the $\mathbf{e}_i$ position, and S is the cell surface area.

According to Y. Feng et al. MSCs, after priming by myeloma cells, stimulate FAK activation, which improves cell adhesion and cell migration [10]. Additionally, K. Podar et al. studied cell migration under different VEGF and FN concentrations through a transwell migration assay, observing a linear increase in the cell's velocity with the increase of both concentrations [7]. We here consider the effects of the CAFs on cell migration through the effects of the expression of VEGF. Thus, we consider a modulated effect on the number of available receptors of the cells, n_r, due to the VEGF concentration in the ECM, as:

$$n_r = n_{ref} \; \frac{Q_V}{Q_V^0}, \tag{2}$$

where n_{ref} are the receptors of the cell of reference. Q_V and Q_V^0 are the VEGF concentration and the maximum reference VEGF value, respectively. Both parameters, Q_V and Q_V^0, were calibrated considering the VEGF and FN concentrations, and the output velocity obtained experimentally *in-vitro*. In this sense, Q_V corresponds to the VEGF concentration in the referenced *in-vitro* experiments, while Q_V^0 is an auxiliary parameter for the nondimensionalization of Q_V [7].

Cell migration is considered a result of the equilibrium of the forces acting on the cell, which include traction forces, $\mathbf{F}_{trac}$, protrusion forces, $\mathbf{F}_{prot}$, and drag forces, $\mathbf{F}_{drag}$. In this case, the inertial forces are neglected due to the scale of the problem.

In this model, we considered protrusion forces, $\mathbf{F}_{prot}$ due to the spontaneous generation of protrusions in the cell membrane. This force is proportional to the traction forces and is considered by the action of uncontrolled polymerization of actin filaments. Thus, it is defined as a random force as [28,30]:

$$\mathbf{F}_{prot} = \| \mathbf{F}_{trac} \| \; \kappa_{rnd} \; \mathbf{e}_{rnd}, \tag{3}$$

Table 1
Mechanical parameters considered in the model.

Parameter	Description	Value	Ref.
κ	Binding constant	10^8 mol^{-1}	[37,38]
n_{ref}	Number of available receptors	1×10^5	[44,45]
ψ	FN concentration	10–100 ng/mL	[7]
ν_f	ECM viscosity	1.0 kPa s	[46,47]
E_{msc}	MSC stiffness	670 Pa	[10,11]
E_{caf}	CAF stiffness	1500 Pa	[10,11]
E_{mmc}	MMC stiffness	320 Pa	[10,11]
E_{ECM}	ECM stiffness	400 Pa	[46]
t_{min}	Natural time of maturation without stimulus	60 h	[48]
t_p	Time proportional to the mechanical signal of the cell	17 h	[49]
Q_I^0	IGF-1 reference concentration value	10 ng/mL	[12]
Q_V^0	VEGF reference concentration value	30 ng/mL	[7]
Q_T^0	Minimum threshold concentration of TGF-β for CAF differentiation	50 ng/mL	–

where κ_{rnd} and $\mathbf{e}_{rnd}$ are random scalar value ($0 < \kappa_{rnd} < 1$) and unit vector to define the magnitude and direction of the resultant random force, respectively.

Drag forces are defined as opposing forces to a spherical object moving at a velocity $\mathbf{v}_{cell}$ in a medium with ν_f viscosity as [28,31]:

$$\mathbf{F}_{drag} = 6\pi\ r\ \nu_f\ \mathbf{v}_{cell}, \tag{4}$$

where r is the cell radius. Consequently, the force balance on the cell can be represented by [28,31]:

$$\mathbf{F}_{trac} + \mathbf{F}_{prot} + \mathbf{F}_{grav} = \mathbf{F}_{drag}. \tag{5}$$

2.2. Modeling of cell proliferation

Mechanical conditions of the ECM are shown to play a key role in different cellular processes such as differentiation [50–52], maturation [53–55], and apoptosis [56–58]. Thus, the cell Maturation Index (MI), referred to the cell-cycle progression, is a time-dependent process in which the cell evaluates and responds to the specific mechanical and chemical conditions to which it is subjected [55,58]. It can be defined as [28,59]:

$$\mathrm{MI} = \begin{cases} \frac{t}{t_{mat}} & t < t_{mat} \\ 1 & t \geq t_{mat} \end{cases} \tag{6}$$

where t is the cell-cycle progression time, and t_{mat} is the time needed for the cell to complete the cell cycle [31]. The effects of the mechanical conditions, which can increase the rate of cell-cycle progression, are dependent on the cell's internal deformations [26]. So, the cell cycle time is dependent on the mechanical stimuli perceived by the cell at each time, t, which can be defined as:

$$t_{mat} = \left[t_{min} + t_p \gamma_c(t)\right]\ 0.5\ \frac{Q_I}{Q_I^0}, \tag{7}$$

where t_{min} is the minimum time needed for a complete cell-cycle progression, t_p is the time proportionality related to the mechanical signal $\gamma_c(t)$ perceived by the cell. Q_I and Q_I^0 correspond to the IGF-1 concentration and the maximum IGF-1 reference concentration value, respectively, which represents the chemical stimuli of the MMCs [12,60]. In this sense, according to M. Zlei et al. Q_I was established as the IGF-1 concentration in their experiments. Consequently, Q_V^0 has been calibrated to obtain proliferation enhancement comparable to their results [12].

The mechanical signal of the cell is obtained from the mean cell's internal deformations such as [28]:

$$\gamma_c(t) = \frac{1}{n} \sum_{i=1}^{n} \mathbf{e}_i : \epsilon_i : \mathbf{e}_i^T, \tag{8}$$

being ϵ_i the strain tensor at each membrane node, ith, of the cell. $\mathbf{e}_i$ is the director unit vector of each membrane node towards the cell centroid.

2.3. CAF differentiation

Ridge et al. in their interesting review, pointed out that TGF-β plays a major role in the transition from MSCs to CAFs [8]. In this sense, several authors have studied how MSCs transitions into CAFs when exposed to TGF-β. Thus, the differentiation of MSCs into CAFs is conditioned by the state of maturation (MI) as well as the level of TGF-β concentration. Hence, once the MSCs reach a complete cell cycle, i.e. MI=1, and the minimum threshold of TGF-β stimulation is achieved, MSCs differentiate into CAF phenotype. So, it can be defined as:

$$\mathrm{MSC} = \begin{cases} \mathrm{CAF} & Q_T^0 \leq Q_T\ \&\ \mathrm{MI} = 1 \\ \text{no differentiation} & \text{Otherwise} \end{cases} \tag{9}$$

where Q_T and Q_T^0 are the concentration and minimum threshold concentration of TGF-β for CAF differentiation, respectively. Although this relationship has been reported by numerous authors, to the authors' knowledge, there is no report from which these parameters can be obtained directly. In this sense, without prejudice to the results, certain predicted values have been suggested for this process.

2.4. Model assumptions

Some assumptions have been taken into account in order to reduce the model's computational cost. In this sense, cell geometry is considered spherical with no changes in its morphology [61]. To represent cells, a constant diameter of 15 μm is considered for all cells, even some differences in cell diameter between cell types can be found in the bibliography [32,62–64]. In general, cell properties are considered homogeneous for every cell phenotype. However, slight discrepancies can be found due to the non-homogeneous nature of MMCs, MSCs, and CAFs [12]. Due to the lack of *in-vitro* experiments, the MSC differentiation threshold, as well as CAFs and MMCs cytokine and factors expression, has been estimated [8,10,11,60]. Finally, neither oxygen nor nutrient consumption has been considered in this study. All the model parameters can be found in Table 1.

3. Results

To describe and validate each cell's response to the considered factors, we have prepared a series of computational experiments, which have been compared with *in-vitro* results in the bibliography. In the first case, we studied the effect of different concentrations of IGF-1 on MMCs proliferation. Secondly, the enhancement of the mechanical ability of MMCs due to the presence of VEGF, as well as the effects of the FN concentration in the ECM, has been studied. Later, we investigated MSC differentiation into CAF due to the TGF-β stimulation. Finally, different coupled effects have been analyzed with the proposed model, where gradients for the different factors, and the presence of MMCs and MSCs or CAFs, have been considered (see Fig. 1).

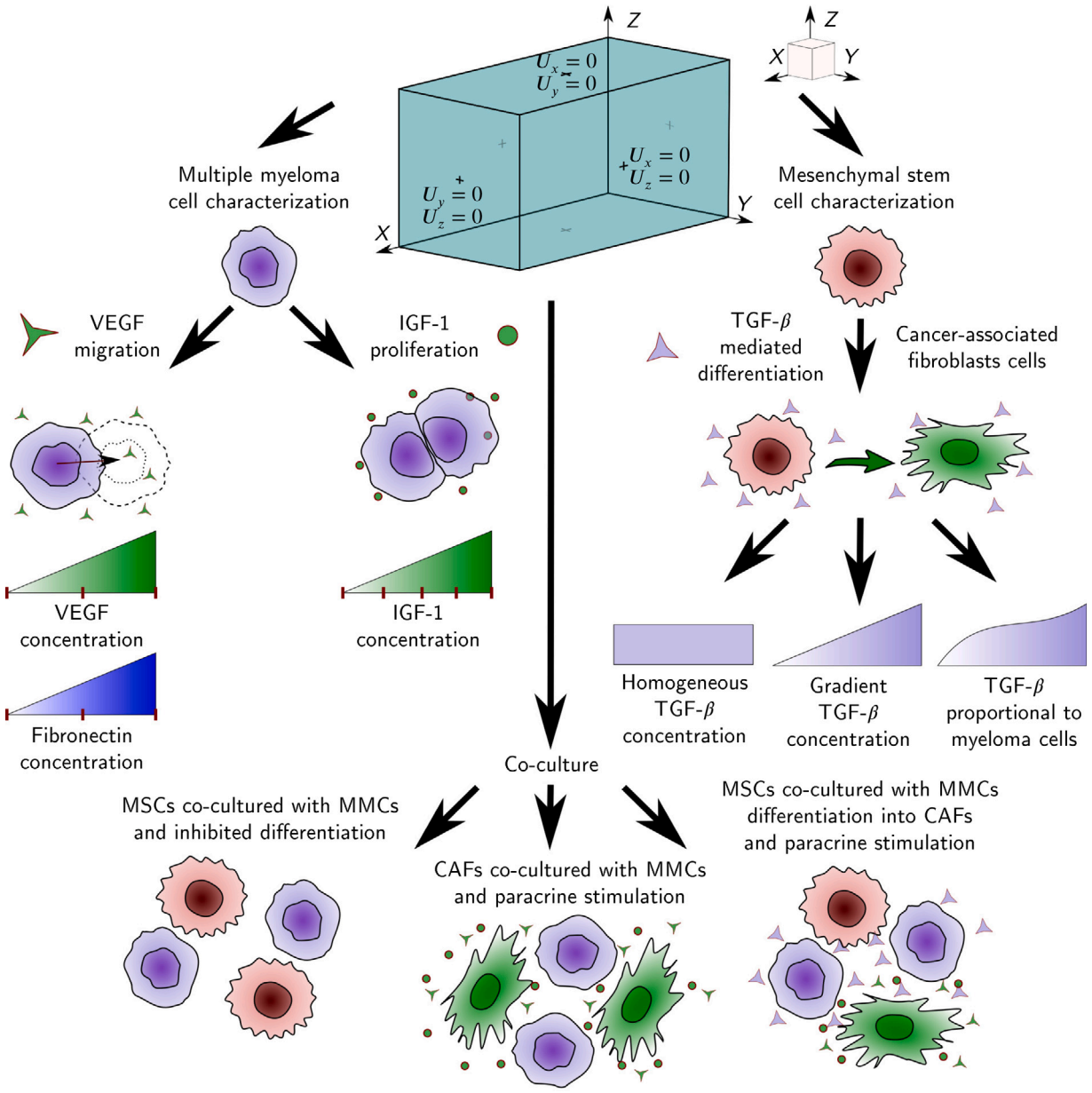

Fig. 1. Graphical representation of the overall study presented with the developed model.

3.1. Stimulation of MMCs proliferation via IGF-1

To validate the model, a series of numerical experiments have been prepared by considering different distributions of IGF-1 ranging from 0 to 15.0 ng/mL. Each experiment was repeated five times for different random initial cell distributions with different random initial cell MI. The model validation was studied through two control experiments, with 0.0 and 10.0 ng/mL IGF-1 concentrations, during six days. Later, a parametric study of the effect of different IGF-1 concentrations was performed.

The results were qualitatively consistent with the *in-vitro* experiment of reference (Fig. 2(a)) [12]. The results show that cell proliferation increased as the IGF-1 concentration was increased. After 24 h, the cells migrated to the central area of the ECM guided by the stiffness of the ECM and the presence of other nearby cells. The cells in contact decreased their internal deformation, increasing the rate of cell maturation and hence cell proliferation. Thus, cells in the inner part of the cell aggregates showed faster maturation. In the control experiment (non-stimulated), after 24 h, a total of 60–64 cells was observed, which increased to 127–158 cells after 96 h (Fig. 3). For the 10.0 ng/mL concentration, after 24 h, a total of 65–88 cells was found, which increased to 203–243 cells after 96 h. These results correspond to a 3.31 ± 0.36 and 5.19 ± 0.47 in cell doubling (number of cells to the initial cell number) after 96 h, for the control and maximum IGF-1 concentration, respectively. Once reach 10.0 ng/mL, a saturation stimulus was considered, and no significant increase in cell proliferation was observed for 15.0 ng/mL (Fig. 2 (b)). Increased variability was observed at 96 h, when the effects of the internal deformations and IGF-1 stimulation on cell proliferation, were accumulated over the simulated time.

3.2. Effect of VEGF and FN interaction in MMCs migration

Cell traction forces, and thus cell motility, are improved with the presence of VEGF in a dose-dependent manner, while it is proportional to the FN concentration in the ECM. Thus, to validate the model, a series of computational experiments were performed for 0, 50, and 100 ng/mL concentrations of VEGF, in an ECM with 0, 50, and 100 ng/mL

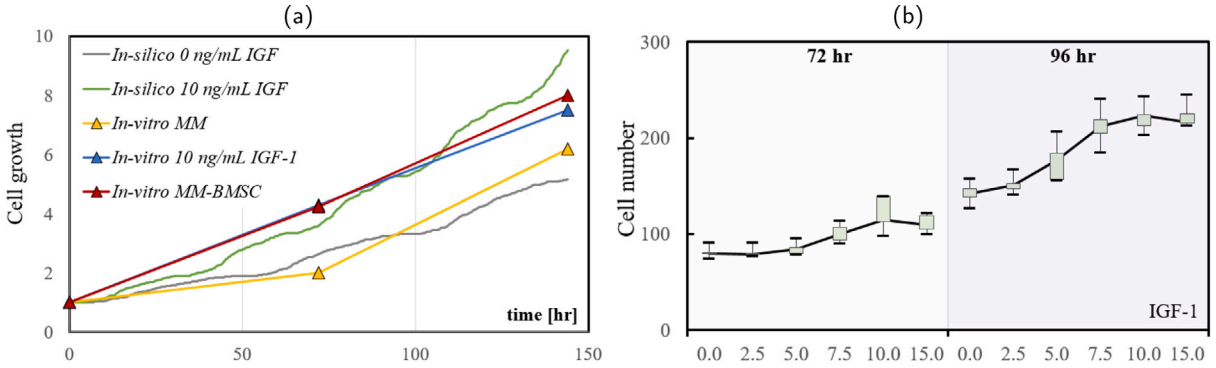

Fig. 2. Cell growth (doubling number) for different IGF-1 concentrations. (a) Validation of the cell doubling number results for six days of simulation. Control case (0 ng/mL of IGF-1) and 10.0 ng/mL IGF-1 concentration was compared with *in-vitro* results [12]. (b) Variation of the cell proliferation for 72 and 96 h with the IGF-1 concentration. The results showed faster cell maturation, which increased cell proliferation. After 72 h, a slight effect on the cell proliferation was observed linearly dependent on the IGF-1 concentration. After 96 h, cell proliferation was doubled compared with the non-stimulated case.

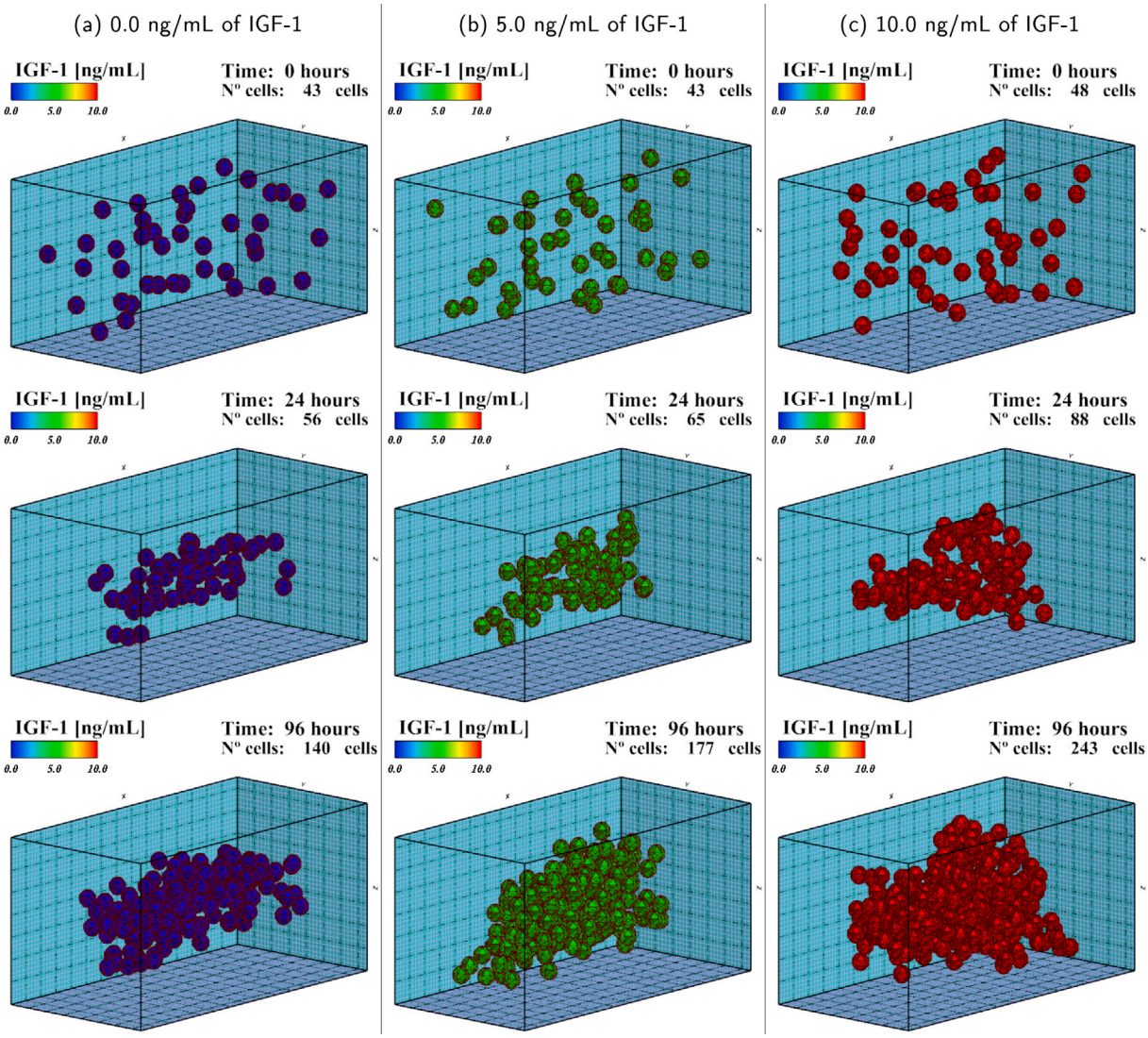

Fig. 3. Stimulation of MMCs proliferation via different IGF-1 concentrations. (a) Control experiment (non-stimulated). After 24 h, cells migrated towards the central zone of the ECM where cells proliferated. After 96 h, cells continued proliferating to reach a total of 127–158 cells. (b) Experiment for 5.0 ng/mL concentration. After 24 h, a slight increase in cell number was observed. After 96 h, cell proliferation increased 24.65% as compared with non-stimulated cells, reaching a total of 156–207 cells. (c) Experiment for 10.0 ng/mL concentration. Cells showed the fastest maturation due to the maximum IGF-1 stimulation. After 96 h, cell proliferation increased 57.04% as compared with non-stimulated cells reaching a total of 203–243 cells (See also Video S1).

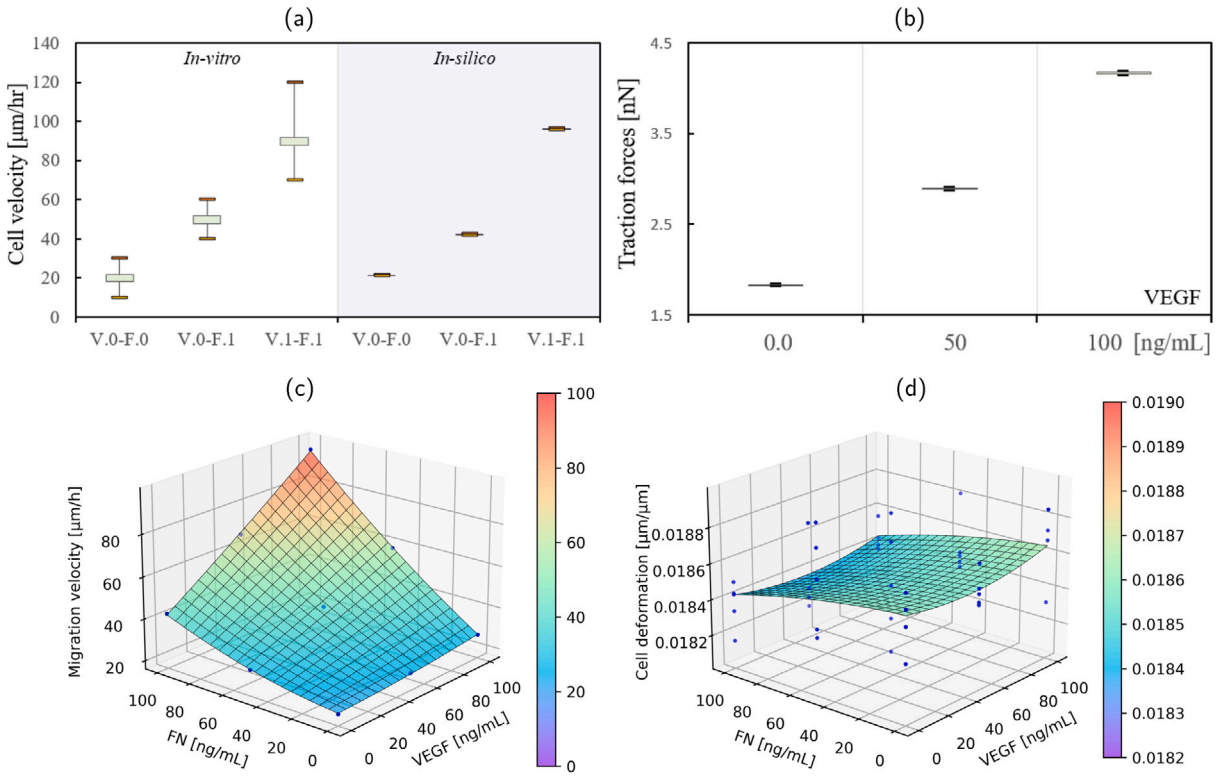

Fig. 4. Results for different VEGF and FN concentrations. (a) Mean cell velocity compared with the *in-vitro* results corresponding to 10 ng/mL of FN (V.0-F.0), 100 ng/mL of FN (V.0-F.1), and 100 ng/mL of both VEGF and FN (V.1-F.1) [7]. (b) Results for mean cell traction forces corresponding to 0 ng/mL, 50 ng/mL, and 100 ng/mL of VEGF, with 100 ng/mL of FN for all cases. VEGF enhanced the capacity of the cells to interact with the FN within the ECM. Besides, an increase in the FN concentration increased the traction forces developed by the cells. (c) Results for mean cell migration velocity. Cell migration velocity increased proportionally to the VEGF and FN concentration. (d) Results for mean cell internal deformation. Cell internal deformations were decreased as the FN concentration increased. Slight differences can be observed with VEGF variation.

concentrations of FN. Each computational experiment was repeated for five random initial cell distributions with random initial MI. The results of these experiments were compared with *in-vitro* experiments in the bibliography [7].

Results were in good qualitative agreement with *in-vitro* reference experiments (Fig. 4(a)) [7]. The results show that cell traction forces and, consequently, cell migration velocity, were linearly influenced by FN and VEGF concentrations (Fig. 4(b), (c)). Cells migrate towards the central zone of the ECM guided by its stiffness and by the presence of other surrounding cells. Higher VEGF stimulation resulted in higher cell velocity, which, in turn, increased cell packing and reduced cell internal deformation (Fig. 4(c), (d)). Once cells interacted with other cells, they tended to adhere and stay attached to the neighbor cells. As cells proliferate, new cells incorporated forming cell aggregates (see Fig. 5). These interactions reduced cell internal deformations due to the cell–cell contacts (Fig. 4(d)). However, differences in the mechanical stimulation due to the internal deformation were limited, and no significant differences in cell proliferation were observed after 96 h.

3.3. MSC differentiation into CAF due to the MMCs paracrine effect

To the knowledge of the authors, there are no specific studies that deal with this behavior. Therefore, without prejudice to the outcome, the authors proposed a specific threshold, which can be adjusted once *in-vitro* results are available. Three different configurations were evaluated to consider MSCs differentiation into CAFs. In the first case, a constant concentration of TGF-β in the ECM, which corresponds to the threshold of MSC to CAF differentiation, was considered (Fig. 6(a)). Additionally, a TGF-β gradient distribution from 0 to 100 ng/mL along x-axis, was considered (Fig. 6(b)). Finally, the expression of the TGF-β, proportional to the MMCs number, was studied (Fig. 6(c)).

Once MSCs mature, if the minimum TGF-β threshold was established, cells differentiated into CAF. This process depended on the distribution of this factor in the ECM. For the constant concentration case, cells differentiated once they complete their first cell cycle (Fig. 7 (a)). In the gradient TGF-β case, cells differentiated according to their position in the ECM (Fig. 7(b)). In the last case, as the TGF-β expression from the MMCs was considered, MMCs needed to proliferate and increase their number to achieve the minimum TGF-β threshold (Fig. 7(c)). In this sense, the authors propose both the minimum TGF-β threshold and the TGF-β rate expression. However, once *in-vitro* experiments are available, both parameters can be adjusted to their results. At the end of the simulations, CAFs were located in the inner part of the cell aggregates. This is a result of differences in cell behavior and mechanical properties for the different cell types. This is consistent with *in-vitro* results, where different cell populations tend to reorganize into organoid-like structures [14,65,66].

3.4. MSC-MMC and CAF-MMC interactions

CAF plays a key role in cancer progression, promoting favorable conditions in the ECM for cancer cell growth, homing, and cell survival [69]. In this final section, we contrast the effects of IGF-1 and VEGF expression on CAF enhancement in the presence of MSC. Three different configurations were proposed. In the first one, MMCs were considered co-cultured with CAFs (MMC–CAF) (Fig. 8(a)). In the second case, MMCs were considered co-cultured with MSC cells (MMC–MSC), being inhibited their differentiation due to the TGF-β. According to Lambert et al. this can be achieved by restoring TGF receptor expression in myeloma cells [9]. In the last configuration, MMCs were considered co-cultured with MSC cells. In this case, MSCs differentiate into CAFs according to the TGF-β concentration (MMC-dCAF). In all the cases, IGF-1 and VEGF concentrations were considered proportional to the

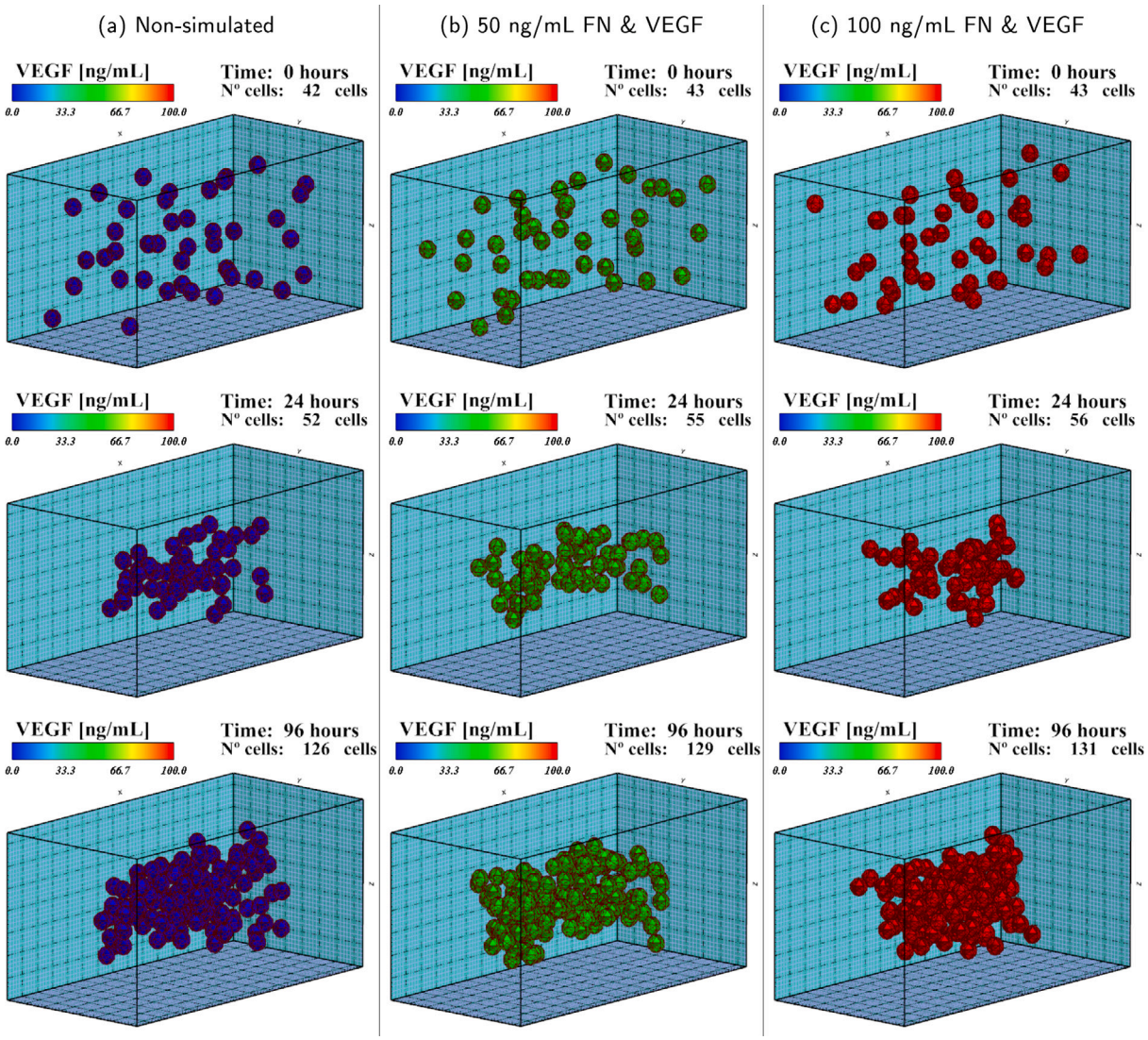

Fig. 5. Effect of VEGF and FN interaction in MMCs migration. Cells migrated towards the central zone of the ECM guided by the ECM stiffness and the presence of other surrounding cells. (a) Control experiment (non-stimulated) for 10 ng/mL concentration of FN with no VEGF stimulation. After 96 h, the cells formed a spherical aggregation in the central area of the ECM. (b) Experiment for 50 ng/mL concentration of FN and 50 ng/mL concentration of VEGF. Faster cell migration was observed due to the combined effect of the FN and VEGF. (c) Experiment for 100 ng/mL concentration of FN and 100 ng/mL concentration of VEGF. After 24 h, higher cells' packing was observed compared with lower FN and VEGF stimuli, which results in higher compaction after 96 h (See also Video S2).

number of CAFs, while TGF-β concentration was proportional to the number of MMCs. Thus, the incidence of their effects were applied progressively as their concentration were increased. As in the previous cases, 40–45 cells were randomly seeded in the ECM with random initial MI. In this experiments, 18–20 cells were considered MSC or CAF, depending on the case of study, and 22–25 cells were considered MMCs. Initially, all the cytokine and factors concentrations were 0 ng/mL and scaled with the number of CAFs and MMCs. Each case was repeated five times with different initial cell distributions to compare the variability of the results.

The results showed that MMCs stimulated by CAFs increased their proliferation due to the expression of IGF-1 (Fig. 8(a)). In comparison, MMCs stimulated by MSCs, showed less cell growth after 96 h (Fig. 8(b)). When differentiation of MSCs was considered in MMCs stimulation, cell proliferation, and motility improvement were delayed until MSCs were differentiated (Fig. 8(c)). Due to differences in proliferation rates between CAFs and MSCs, the final number of CAFs in the MMC-dCAF case was higher than the MMC–CAF, and thus, higher were the stimuli of IGF-1 and VEGF. After 24 h, in the case of MMC–CAF, a slight improvement in cell proliferation was observed compared with MMC–MSC and MMC-dCAF (Fig. 9(a), (b)). However, these differences highly increased after 96 h, where the number of CAFs was higher and, consequently, the produced stimulus. This tendency was also observed in the traction forces (Fig. 9(c)) and cell migration velocity (Fig. 9(d)), which was proportional to the traction forces. After 96 h of MMC–CAF interaction, the concentration of IGF-1 and VEGF reached 6–7 ng/mL and 70–80 ng/mL, respectively, while null cytokine and factors concentrations were considered in the MMC–MSC case (Fig. 8).

4. Discussion

Zlei et al. studied MMCs growth stimulated by 3 different cytokines and factors combinations [12]. These stimuli, which include IL-6, IGF-1, VEGF, and SDF-1 are present in the BM and are expressed by the MSC [3,8]. They observed that, under IL-6, SDF-1, and IGF-1 stimulation, cell proliferation, and cell viability increased. According to the general consensus, IL-6 is mainly involved in cell survival and the development of drug resistance, while SDF-1 was reported to play a key role in metastasis and homing of MMCs [13,67]. In this sense, in order to define separately their effects, we considered proliferation enhancement due

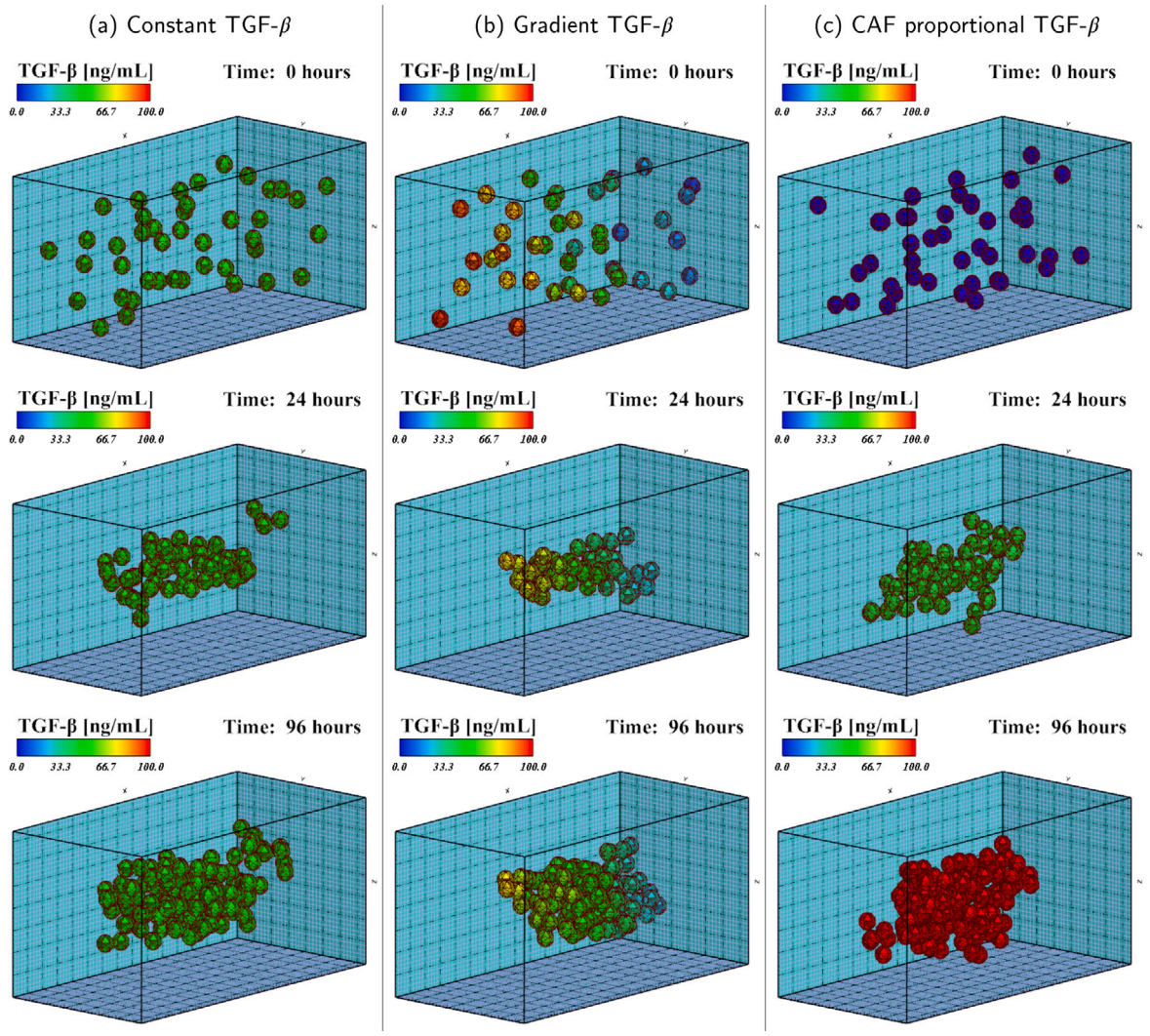

Fig. 6. MSCs differentiation into CAFs due to the MMCs paracrine effect. (a) Constant homogeneous distribution of TGF-β. (b) Gradient distribution of TGF-β (0–100 ng/mL) in the longitudinal direction. (c) TGF-β proportional to the number of MMC (See also Video S3).

to the IGF-1, while a combination of different factors could be also assumed.

The results of the computational model are in agreement with their results (Fig. 2). Thus, cell proliferation increased as the IGF-1 concentration increased. The model assumes a saturation point for the IGF-1 stimulus. After this point, higher IGF-1 concentrations do not increase cell proliferation. Below this saturation level, linear stimulation has been considered. However, the results show a non-linear relationship between the IGF-1 concentration and the cell number. In this sense, the effect of other stimuli may be acting simultaneously. The cells' internal deformation was also evaluated, which showed a decrease when the IGF-1 stimulus increased. These cell internal deformations were related to the cell distribution in the matrix and the degree of compaction of the cells. Thus, as the cell proliferation increases, due to the IGF-1 concentration, cell packing was augmented, which increased, even more, cell proliferation due to the mechanical stimulation of the cells. In this sense, the non-linear effect was associated with the coupled effects of the IGF-1 and mechanical stimuli (see Fig. 3). For the 10 ng/mL concentration of IGF-1, the results showed a huge increase in the cells after 144 h, which was attributed to the high concentration of the cells at the end of the simulations (see Fig. 2(a)). In contrast, the non-stimulated cells continue with a slight increase in the cell numbers. In this sense, the mechanical stimulation was cumulative over the time of simulation, showing higher differences in long simulated times. After this point, due to the limitations in the considered ECM dimensions, the cells stopped their proliferation and the results were no longer representative (data not shown). Additionally, even though their effects are hidden, space limitations within cell aggregates reduce the rate of proliferation through contact inhibition [68].

VEGF plays multiple roles in cancer progression, such as angiogenesis, metastasis, and homing [3,7,69]. S. Ridge et al. reported that BM cells migrate to pre-metastatic sites before tumor cells arrive, and, by blocking the VEGF-receptor, this cluster formation and metastasis can be inhibited [8]. In this sense, K. Podar et al. studied the effect of VEGF on MMCs migration observing that cell migration velocity were proportional to the VEGF and FN concentrations [7]. Moreover, VEGF was associated with an increase in FAK activation, which enhanced cells' adhesion to the FN fibers, increasing migration speed and guiding the cells along the fibers direction. In the computational model, a linear increase of cell traction forces can be observed as the concentrations of VEGF and FN are increased, which in turn increases cell migration velocity (Fig. 4). The coupling effect of FN and VEGF was higher than the individual contribution of each stimulus separately. When compared to the non-stimulated or minimum FN case, the increase of the FN represents an increase in cells' velocity. It was 21.49 μm/h for the minimum FN concentration, while it was 42.21 μm/h for maximum concentration (mean values). On the other hand, the effect of the VEGF stimulus when combined with minimum increased the cells' velocity to

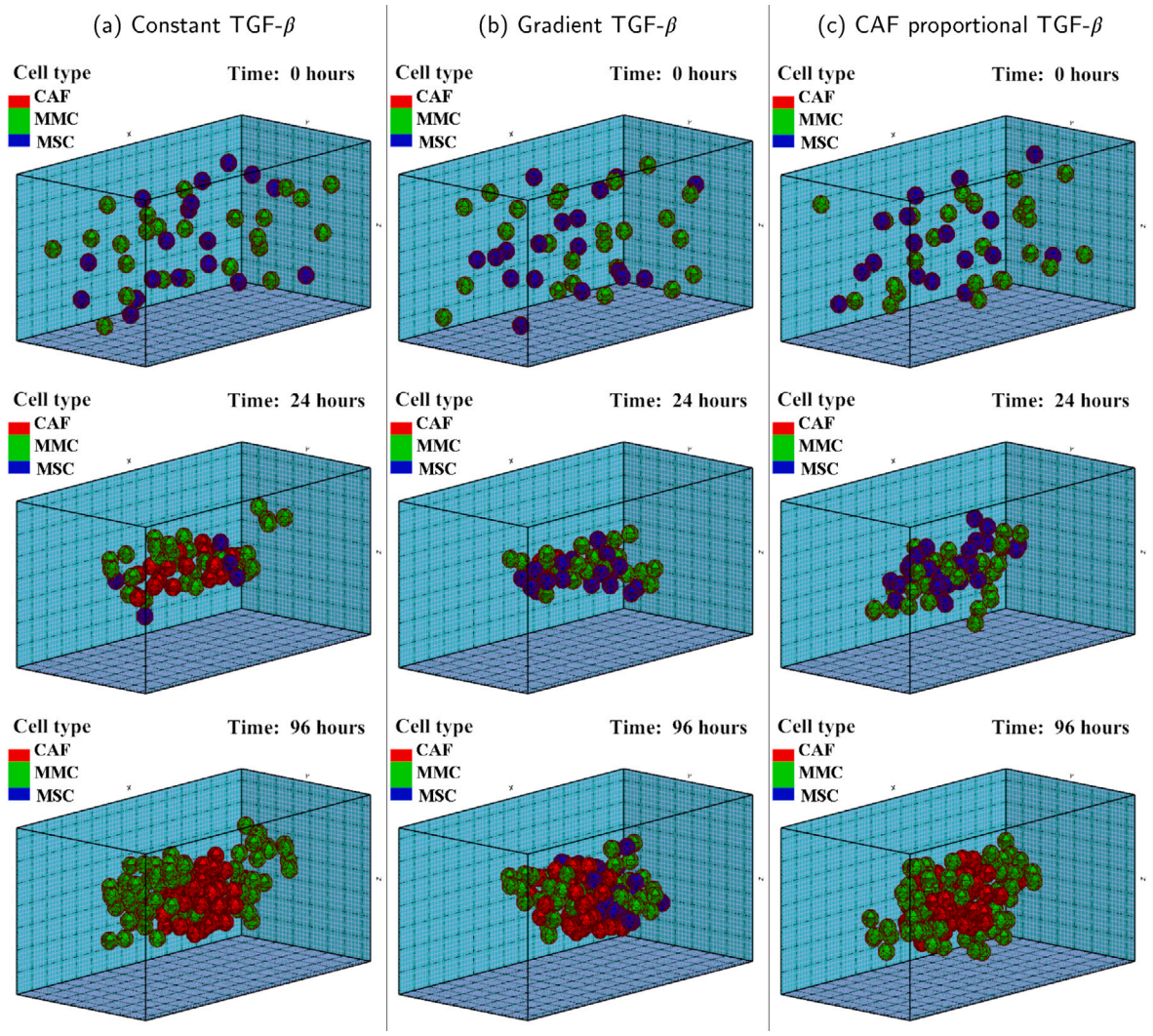

Fig. 7. MSC differentiation under different TGF-β stimulus.(a) After 24 h, with a constant distribution of TGF-β, cells started to differentiate. After 96 h, all MSCs were differentiated into CAFs and migrated towards the inner part of the cell aggregation. (b) After 24 h under a gradient distribution of TGF-β, cells in the higher concentration zones started to differentiate. After 96 h, differentiated CAFs were in the inner part of the cell aggregation, while some MSCs, in lower TGF-β concentration, were still undifferentiated. (c) After 24 h with TGF-β stimulus proportional to the number of MMC, MSCs were still undifferentiated. After 45–50 h, due to the MMCs proliferation, TGF-β concentration reached the CAF differentiation threshold and MSCs started to differentiate. After 96 h, all the MSCs were differentiated into CAFs (See also Video S4).

27.33 μm/h. The accumulated effect of both maximum concentrations increased the cells' migration velocity to 96.03 μm/h. Thus, the individual effects of the FN and VEGF concentration increased by 0.96 and 0.27 times with respect to the non-stimulated case, respectively, while the combined effect rose to 3.47 times concerning the non-stimulated.

The effect of these stimuli was to increase the velocity at which cells made contact. This results in a slightly induced mechanical stimulation due to the reduction of the cell's internal deformation. However, even though the cells migrate faster, this does not ensure higher packing. Thus, the reduction of the cell's internal deformation was lower than in the previous case (IGF-1 stimulation), and differences in cell proliferation were negligible. When compared to *in-vitro* results, there were significant differences in the variability of the cells' migration velocities (see Fig. 4(a)). These differences were attributed to the heterogeneity of the cells in the *in-vitro* experiments, while the properties and geometry of the *in-silico* cells are considered homogeneous.

CAFs are considered as the major contributor to the tumor microenvironment, such that they improve cell proliferation, induce angiogenesis, promote cell survival, and activate cell invasion through paracrine signaling [70–72]. Their origin is heterogeneous, which include multiple progenitor cell types, such as epithelial cells, MSC, and fibroblasts [8,14]. Among these cells, S. Ridge et al. pointed to MSCs as a source for CAFs, where TGF-β, among other factors, could contribute triggering this differentiation [8]. Besides, other authors observed that blocking TGF-β inhibit MSCs upregulation of proliferation, migration and invasion in various cancer cells [8,73]. These findings were consistent with those of D. Saforo et al. who observed that tumor-derived cells cultured in 3D hypoxic conditions, where TGF-β showed the maximum expression, alter their phenotype to produce pro-tumorigenic factors [70]. Other authors report that TGF-β plays a dual role in cancer progression, with suppressive effects in the early stages of cancer development but promoting metastasis in the late stages [8,9,14,74]. In this sense, the differentiation of MSCs into CAFs, induced by TGF-β, could be responsible for this phenomenon. While cells expressing the MSC phenotype that may have a tumor-suppressive response, CAFs exhibit pro-tumor behavior. In this sense, D. Wu et al. observed that the stiffness of myeloma cells increased significantly due to their interactions with myeloma patient-derived MSCs, compared with those co-cultured with normal MSC [10]. In this model, the authors propose MSC differentiation under a determined TGF-β concentration. This concentration threshold was established by the authors due to the lack of experimental data in this regard. As cells perceive the TGF-β with concentrations higher than the minimum threshold, they trigger CAF differentiation. In locations where the minimal concentration of TGF-β

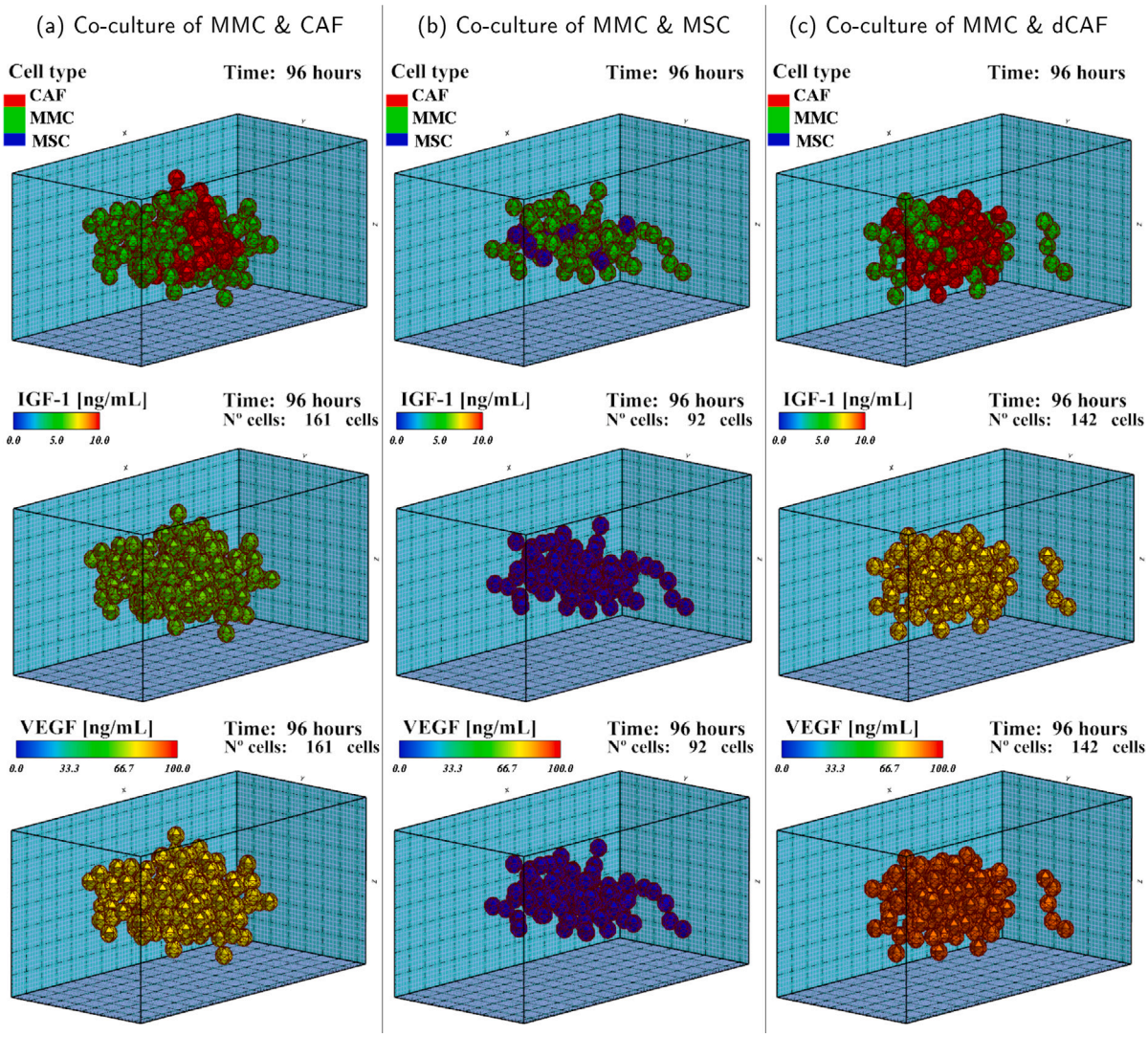

Fig. 8. MMCs interactions with CAFs and MSCs after 96 h. (a) Co-culture of MMCs with pre-differentiated CAFs. (b) Co-culture of MMCs with MSCs in which TGF-β effect was inhibited. (c) Co-culture of MMCs with MSCs, which differentiated into CAF phenotype due to the presence of TGF-β. CAFs expressed IGF-1 and VEGF, which improved cell proliferation and cell motility. Their concentrations were dependent on the number of CAFs in the ECM (See also Video S5, Video S6, and Video S7).

is unavailable, MSCs remain undifferentiated. Thus, different configurations of the TGF-β concentration were proposed, observing relevant differences in cells differentiation. Cells under non-homogeneous TGF-β concentration differentiate in zones where this concentration exceeds the minimum threshold. As the TGF-β was considered to be expressed by cancer cells, we considered TGF-β concentration proportional to the number of myeloma cells. Consequently, it can be possible to study differences in tumor growth with different cancer cells and MSCs proportionalities, which showed relevant differences in cancer behavior [75]. At the start of the simulation, with few MMCs, MSCs retain their normal phenotype. As MMCs proliferate, the TGF-β concentration increases which triggers MSCs differentiation into CAFs. In a real tumor microenvironment, different cells located in different positions can perceive a variety of conditions, resulting in non-homogeneous behaviors.

As the considered cytokines and factors are expressed by the different cells in the tumor microenvironment, their concentrations in this computational model depend on the number of cells expressing them. In this sense, we established proportional concentrations of the different cytokines in a computational experiment where all the stimuli were acting simultaneously (Fig. 8). Under these conditions, we studied MMCs growth in co-cultures of CAF and MSC. An increase in cell proliferation and cell forces were observed under IGF-1 and VEGF stimulation produced by the CAF cells. MSCs differentiation into CAFs also depended on the number of MMCs in the ECM. When inhibition of the TGF-β was considered, even though the MMCs continue increasing, and thus the TGF-β concentration, differentiation of MSCs was not triggered. In this case, the upregulation of proliferation and migration was also inhibited (see Fig. 9). Differences between the initial consideration of CAFs (MMC–CAF) and the differentiation of MSCs (MMC-dMSC) were also observed. As MSCs proliferate faster, at the end of the simulation, a higher number of differentiated CAFs were observed compared to CAFs in MMC–CAF case. Thus, the final concentration of VEGF and IGF-1, and their effects on MMCs, were also higher.

The results showed interesting differences in co-culture experiments. Different characteristics make cells behave in different ways. When MMCs are co-cultured with MSCs and CAFs, their differences in mechanical properties (see Table 1) cause them to be positioned differently in the ECM (see Figs. 7 and 8). MSCs and CAFs were 2.1 and 4.7 times stiffer than MMCs, respectively, which improves their capacity to interact with the ECM. At the end of the simulations, CAFs and MSCs are located in the inner part of the cell's aggregates, while the MMCs are distributed at the periphery. This is in accordance with *in-vitro* findings where a correlation between the cell phenotype and their location was observed [65,66]. This was reported by R. Foty in

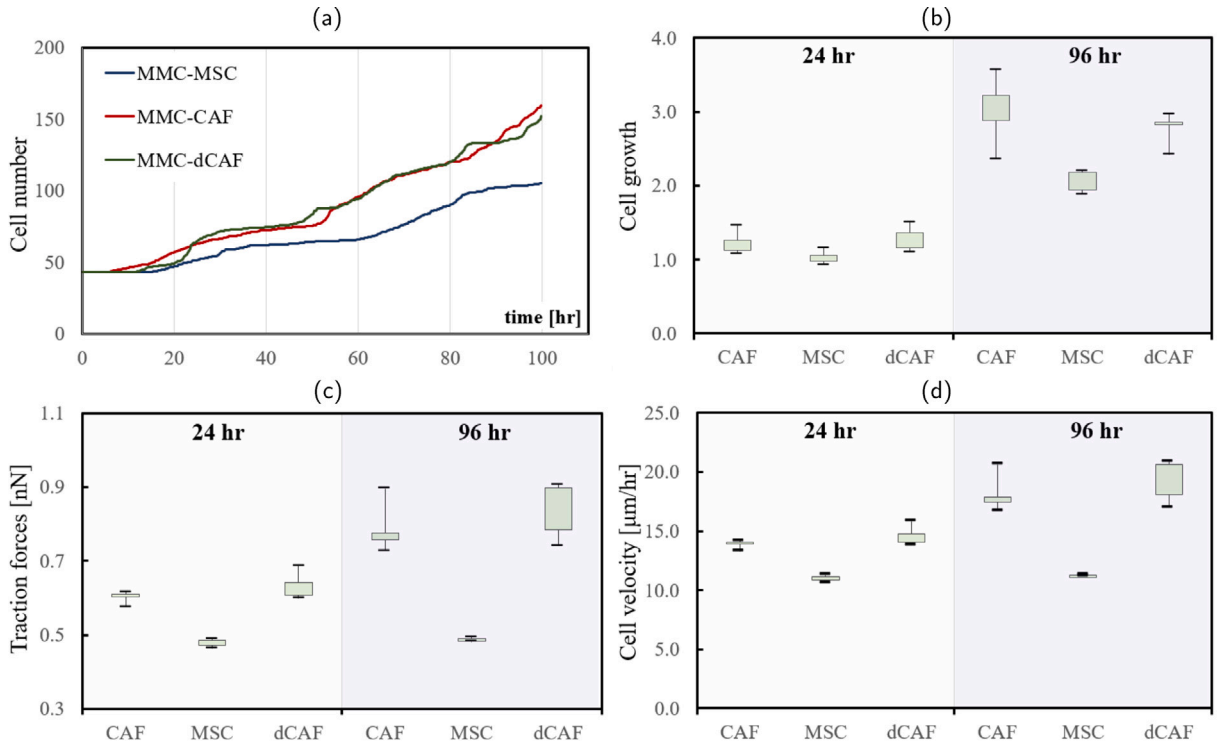

Fig. 9. Results of MMC–MSC and MMC–CAF interaction. (a) Cell proliferation and (b) cell doubling number. Cell proliferation was increased when considered CAFs stimulation. The effect was increased after 96 h where higher IGF-1 concentration was observed. (c) Traction forces and (d) mean cell migration velocity. Cell forces and cell migration were increased due to the expression of VEGF by the CAFs.

co-cultures of heart and liver cells. The heart cells are distributed in the inner part of these aggregates, while the liver cells stay at the periphery [66].

5. Conclusion

We have presented a new computational model to study MMCs behavior and tumor growth. In this model, the effect of the paracrine interactions with MSCs and CAF have been considered in cell growth, migration and differentiation. The model couples the effect of the mechanical cues with the cell response to different cytokines, which directly influence the cells' behavior. The obtained results are consistent with the bibliography [7–12,60,76,77].

In this computational model, myeloma cell growth was increased as a response to the cytokines expressed by CAF cells. IGF-1 increases cell proliferation by reducing the cell cycle of the cells. This effect was coupled with the mechanical stimulation of the cells guided by the ECM stiffness. In this way, a non-linear improvement of the cell proliferation is observed as the IGF-1 stimulus is increased. VEGF, which improved cell adhesion to the ECM fibers, increased cell exerted forces and, thus, cell migration. With this model, the biparametric dependence can be considered and studied in different cell culture conditions. Cells migrated faster towards the central zone of the ECM, which was the stiffest part of the ECM. An increase in the cells packing was observed, with a slight reduction in the cell internal deformations due to the cell–cell interactions. Despite this mechanical stimulation, cell proliferation was not significantly increased. In the presented model, we considered the MSC differentiation due to the MMC interaction. Although we proposed a reference threshold of TGF-β to trigger this differentiation, the model can easily be calibrated to the specific *in-vitro* results when available. So, the authors encourage the experimental colleagues to cover this point. On the other hand, different distributions of TGF-β was taken into account to study cell differentiation. Cells under a higher concentration of TGF-β, which corresponds to a higher concentration of myeloma cells, differentiated faster and started to produce pro-tumor cytokines, which improved MMCs growth, and motility. As a result of differences in the mechanical properties of the cells, their distribution differs according to the cell phenotype. CAFs migrate to the inner part of cell aggregations, while MMCs remain at the periphery. As CAFs differentiated and proliferated, cytokines concentration increased, which increased their pro-tumor effect.

The presented computational model is able to consider a wide range of different complex tumor microenvironments during tumor growth. This includes different cytokine concentrations, multiple simultaneous cell types, with distinct mechanical properties and behavior, and complex mechanical conditions. Even though we estimated some reference values for certain aspects and parameters of the model, such as the different cell type concentrations, differentiation thresholds, and cytokine expression kinetics, these values can be adjusted based on patient-specific data, when available, in order to carry out simulations to study the most effective strategies for cancer treatment. Thus, we considered the presented model as a helpful tool for predicting and a better understanding of the biological interaction between MMCs and resident bone marrow cells.

Declaration of competing interest

The authors declare that they have no known competing financial interests or personal relationships that could have appeared to influence the work reported in this paper.

Acknowledgments

The authors gratefully acknowledge the financial support through the project PID2019-106099RB-C44, funded by MCIN/AEI, Spain/10.13039/501100011033, and the Government of Aragón, Spain (DGA-T24_20R). The authors would like to express their gratitude to the anonymous reviewers for their careful reading and professional comments, which helped improve the manuscript.

Appendix A. Supplementary data

Supplementary material related to this article can be found online at https://doi.org/10.1016/j.compbiomed.2022.106458.

References

[1] G. Gastelum, M. Veena, K. Lyons, C. Lamb, N. Jacobs, A. Yamada, A. Baibussinov, M. Sarafyan, R. Shamis, J. Kraut, P. Frost, Can targeting hypoxia-mediated acidification of the bone marrow microenvironment kill myeloma tumor cells? 2021, http://dx.doi.org/10.3389/fonc.2021.703878.

[2] M. Abe, T. Harada, T. Matsumoto, Concise review: Defining and targeting myeloma stem cell-like cells, Stem Cells 32 (5) (2014) 1067–1073, http://dx.doi.org/10.1002/stem.1643.

[3] S.K. Kumar, V. Rajkumar, R.A. Kyle, M. van Duin, P. Sonneveld, M.-V. Mateos, F. Gay, K.C. Anderson, Multiple myeloma, Nat. Rev. Dis. Primers 3 (1) (2017) 17046, http://dx.doi.org/10.1038/nrdp.2017.46.

[4] K.C. Anderson, R.D. Carrasco, Pathogenesis of myeloma, Annu. Rev. Pathol.: Mech. Dis. 6 (1) (2011) 249–274, http://dx.doi.org/10.1146/annurev-pathol-011110-130249.

[5] L. Perez-Amill, G. Suñe, A. Antoñana-Vildosola, M. Castella, A. Najjar, J. Bonet, N. Fernández-Fuentes, S. Inogés, A. López, C. Bueno, M. Juan, Á. Urbano-Ispizua, B. Martín-Antonio, Preclinical development of a humanized chimeric antigen receptor against B cell maturation antigen for multiple myeloma, Haematologica 106 (1) (2020) 173–184, http://dx.doi.org/10.3324/haematol.2019.228577.

[6] F. Saba, M. Soleimani, S. Abroun, New role of hypoxia in pathophysiology of multiple myeloma through mir-210, EXCLI J. 17 (2018) 647–662, http://dx.doi.org/10.17179/excli2018-1109.

[7] K. Podar, Y.-T. Tai, B.K. Lin, R.P. Narsimhan, M. Sattler, T. Kijima, R. Salgia, D. Gupta, D. Chauhan, K.C. Anderson, Vascular endothelial growth factor-induced migration of multiple myeloma cells is associated with β1 integrin- and phosphatidylinositol 3-kinase-dependent pKCα activation, J. Biol. Chem. 277 (10) (2002) 7875–7881, http://dx.doi.org/10.1074/jbc.M109068200.

[8] S.M. Ridge, F.J. Sullivan, S.A. Glynn, Mesenchymal stem cells: key players in cancer progression, Mol. Cancer 16 (1) (2017) 31, http://dx.doi.org/10.1186/s12943-017-0597-8.

[9] K.E. Lambert, H. Huang, K. Mythreye, G.C. Blobe, The type III transforming growth factor-β receptor inhibits proliferation, migration, and adhesion in human myeloma cells, in: K. Luo (Ed.), Mol. Biol. Cell 22 (9) (2011) 1463–1472, http://dx.doi.org/10.1091/mbc.e10-11-0877.

[10] Y. Feng, G. Ofek, D.S. Choi, J. Wen, J. Hu, H. Zhao, Y. Zu, K.A. Athanasiou, C.-C. Chang, Unique biomechanical interactions between myeloma cells and bone marrow stroma cells, Prog. Biophys. Mol. Biol. 103 (1) (2010) 148–156, http://dx.doi.org/10.1016/j.pbiomolbio.2009.10.004.

[11] D. Wu, X. Guo, J. Su, R. Chen, D. Berenzon, M. Guthold, K. Bonin, W. Zhao, X. Zhou, CD138-negative myeloma cells regulate mechanical properties of bone marrow stromal cells through SDF-1/CXCR4/AKT signaling pathway, Biochim. Biophys. Acta - Mol. Cell Res. 1853 (2) (2015) 338–347, http://dx.doi.org/10.1016/j.bbamcr.2014.11.019.

[12] M. Zlei, S. Egert, D. Wider, G. Ihorst, R. Wäsch, M. Engelhardt, Characterization of in vitro growth of multiple myeloma cells, Exp. Hematol. 35 (10) (2007) 1550–1561, http://dx.doi.org/10.1016/j.exphem.2007.06.016.

[13] R. Bam, W. Ling, S. Khan, A. Pennisi, S.U. Venkateshaiah, X. Li, F. van Rhee, S. Usmani, B. Barlogie, J. Shaughnessy, J. Epstein, S. Yaccoby, Role of Bruton's tyrosine kinase in myeloma cell migration and induction of bone disease, Am. J. Hematol. 88 (6) (2013) 463–471, http://dx.doi.org/10.1002/ajh.23433.

[14] S. Avnet, S. Lemma, M. Cortini, G. Di Pompo, F. Perut, N. Baldini, Pre-clinical models for studying the interaction between mesenchymal stromal cells and cancer cells and the induction of stemness, Front. Oncol. 9 (APR) (2019) 305, http://dx.doi.org/10.3389/fonc.2019.00305.

[15] J. Hu, E. Van Valckenborgh, E. Menu, E. De Bruyne, K. Vanderkerken, Understanding the hypoxic niche of multiple myeloma: therapeutic implications and contributions of mouse models, Dis. Models Mech. 5 (6) (2012) 763–771, http://dx.doi.org/10.1242/dmm.008961.

[16] S. Clara-Trujillo, G. Gallego Ferrer, J.L. Gómez Ribelles, In vitro modeling of non-solid tumors: How far can tissue engineering go? Int. J. Mol. Sci. 21 (16) (2020) 5747, http://dx.doi.org/10.3390/ijms21165747.

[17] D. Huh, G.A. Hamilton, D.E. Ingber, From 3D cell culture to organs-on-chips, Trends Cell Biol. 21 (12) (2011) 745–754, http://dx.doi.org/10.1016/J.TCB.2011.09.005.

[18] A. Carlier, G.A. Skvortsov, F. Hafezi, E. Ferraris, J. Patterson, B. Koc, H. Van Oosterwyck, Computational model-informed design and bioprinting of cell-patterned constructs for bone tissue engineering, Biofabrication 8 (2) (2016) 025009, http://dx.doi.org/10.1088/1758-5090/8/2/025009.

[19] P. Pivonka, S.V. Komarova, Mathematical modeling in bone biology: From intracellular signaling to tissue mechanics, Bone 47 (2) (2010) 181–189, http://dx.doi.org/10.1016/j.bone.2010.04.601.

[20] F. Galbusera, M. Cioffi, M.T. Raimondi, R. Pietrabissa, Computational modeling of combined cell population dynamics and oxygen transport in engineered tissue subject to interstitial perfusion, Comput. Methods Biomech. Biomed. Eng. 10 (4) (2007) 279–287, http://dx.doi.org/10.1080/10255840701318404.

[21] H. Khayyeri, S. Checa, M. Tägil, F.J. O'Brien, P.J. Prendergast, Tissue differentiation in an in vivo bioreactor: in silico investigations of scaffold stiffness, J. Mater. Sci. Mater. Med. 21 (8) (2010) 2331–2336, http://dx.doi.org/10.1007/s10856-009-3973-0.

[22] S. Checa, P.J. Prendergast, Effect of cell seeding and mechanical loading on vascularization and tissue formation inside a scaffold: A mechano-biological model using a lattice approach to simulate cell activity, J. Biomech. 43 (5) (2010) 961–968, http://dx.doi.org/10.1016/j.jbiomech.2009.10.044.

[23] M. Cioffi, J. Küffer, S. Ströbel, G. Dubini, I. Martin, D. Wendt, Computational evaluation of oxygen and shear stress distributions in 3D perfusion culture systems: Macro-scale and micro-structured models, J. Biomech. 41 (14) (2008) 2918–2925, http://dx.doi.org/10.1016/j.jbiomech.2008.07.023.

[24] S. Manzano, R. Moreno-Loshuertos, M. Doblaré, I. Ochoa, M. H. Doweidar, Structural biology response of a collagen hydrogel synthetic extracellular matrix with embedded human fibroblast: computational and experimental analysis, Med. Biol. Eng. Comput. 53 (8) (2015) 721–735, http://dx.doi.org/10.1007/s11517-015-1277-8.

[25] E. Gavagnin, C.A. Yates, Stochastic and deterministic modeling of cell migration, in: A.S.S. Rao, C.R. Rao (Eds.), Handbook of Statistics, Vol. 39, Elsevier B.V., 2018, pp. 37–91, http://dx.doi.org/10.1016/bs.host.2018.06.002, arXiv:1806.06724v2 URL https://linkinghub.elsevier.com/retrieve/pii/S0169716118300075.

[26] P. Urdeitx, M.H. Doweidar, Enhanced piezoelectric fibered extracellular matrix to promote cardiomyocyte maturation and tissue formation: A 3D computational model, Biology 10 (2) (2021) 135, http://dx.doi.org/10.3390/biology10020135, URL https://www.mdpi.com/2079-7737/10/2/135.

[27] S. Soleimani, M. Shamsi, M.A. Ghazani, H.P. Modarres, K.P. Valente, M. Saghafian, M.M. Ashani, M. Akbari, A. Sanati-Nezhad, Translational models of tumor angiogenesis: A nexus of in silico and in vitro models, Biotechnol. Adv. 36 (4) (2018) 880–893, http://dx.doi.org/10.1016/j.biotechadv.2018.01.013.

[28] S.J. Mousavi, M.H. Doweidar, Role of mechanical cues in cell differentiation and proliferation: A 3D numerical model, in: C.M. Aegerter (Ed.), PLoS One 10 (5) (2015) e0124529, http://dx.doi.org/10.1371/journal.pone.0124529.

[29] P. Urdeitx, S. Farzaneh, S.J. Mousavi, M.H. Doweidar, Role of oxygen concentration in the osteoblasts behavior: A finite element model, J. Mech. Med. Biol. 20 (01) (2020) 1950064, http://dx.doi.org/10.1142/S0219519419500647.

[30] P. Urdeitx, M.H. Doweidar, Mechanical stimulation of cell microenvironment for cardiac muscle tissue regeneration: a 3D in-silico model, Comput. Mech. 66 (4) (2020) 1003–1023, http://dx.doi.org/10.1007/s00466-020-01882-6.

[31] P. Urdeitx, M.H. Doweidar, A computational model for cardiomyocytes mechano-electric stimulation to enhance cardiac tissue regeneration, Mathematics 8 (11) (2020) 1875, http://dx.doi.org/10.3390/math8111875.

[32] A. Bouchnita, F.-E. Belmaati, R. Aboulaich, M. Koury, V. Volpert, A hybrid computation model to describe the progression of multiple Myeloma and its intra-clonal heterogeneity, Computation 5 (4) (2017) 16, http://dx.doi.org/10.3390/computation5010016.

[33] S. Göktepe, O.J. Abilez, K.K. Parker, E. Kuhl, A multiscale model for eccentric and concentric cardiac growth through sarcomerogenesis, J. Theoret. Biol. 265 (3) (2010) 433–442, http://dx.doi.org/10.1016/j.jtbi.2010.04.023, arXiv:77954624210.

[34] D. Shao, W.-J. Rappel, H. Levine, Computational model for cell morphodynamics, Phys. Rev. Lett. 105 (10) (2010) 108104, http://dx.doi.org/10.1103/PhysRevLett.105.108104, arXiv:NIHMS150003.

[35] S.J. Mousavi, M.H. Doweidar, A novel mechanotactic 3D modeling of cell morphology, Phys. Biol. 11 (4) (2014) 046005, http://dx.doi.org/10.1088/1478-3975/11/4/046005.

[36] S.J. Mousavi, M.H. Doweidar, Three-dimensional numerical model of cell morphology during migration in multi-signaling substrates, in: C.M. Aegerter (Ed.), PLoS One 10 (3) (2015) e0122094, http://dx.doi.org/10.1371/journal.pone.0122094.

[37] M.H. Zaman, R.D. Kamm, P. Matsudaira, D.A. Lauffenburger, Computational model for cell migration in three-dimensional matrices, Biophys. J. 89 (2) (2005) 1389–1397, http://dx.doi.org/10.1529/biophysj.105.060723.

[38] S.J. Mousavi, M.H. Doweidar, M. Doblaré, Computational modelling and analysis of mechanical conditions on cell locomotion and cell–cell interaction, Comput. Methods Biomech. Biomed. Eng. 17 (6) (2014) 678–693, http://dx.doi.org/10.1080/10255842.2012.710841.

[39] F.O. Ribeiro, M.J. Gómez-Benito, J. Folgado, P.R. Fernandes, J.M. García-Aznar, Computational model of mesenchymal migration in 3D under chemotaxis, Comput. Methods Biomech. Biomed. Eng. 20 (1) (2017) 59–74, http://dx.doi.org/10.1080/10255842.2016.1198784.

[40] H. Yamaguchi, J. Wyckoff, J. Condeelis, Cell migration in tumors, Curr. Opin. Cell Biol. 17 (5 SPEC. ISS.) (2005) 559–564, http://dx.doi.org/10.1016/j.ceb.2005.08.002.

[41] M. Lintz, A. Muñoz, C.A. Reinhart-King, The mechanics of single cell and collective migration of tumor cells, J. Biomech. Eng. 139 (2) (2017) 021005, http://dx.doi.org/10.1115/1.4035121.

[42] M. Makale, Cellular mechanobiology and cancer metastasis, Birth Defects Res. C - Embryo Today: Rev. 81 (4) (2007) 329–343, http://dx.doi.org/10.1002/bdrc.20110.

[43] J. Guck, F. Lautenschläger, S. Paschke, M. Beil, Critical review: Cellular mechanobiology and amoeboid migration, Integr. Biol. 2 (11–12) (2010) 575–583, http://dx.doi.org/10.1039/c0ib00050g.

[44] H. Berry, V. Larreta-Garde, Oscillatory behavior of a simple kinetic model for proteolysis during cell invasion, Biophys. J. 77 (2) (1999) 655–665, http://dx.doi.org/10.1016/S0006-3495(99)76921-3.

[45] S.J. Mousavi, M.H. Doweidar, Numerical modeling of cell differentiation and proliferation in force-induced substrates via encapsulated magnetic nanoparticles, Comput. Methods Programs Biomed. 130 (2016) 106–117, http://dx.doi.org/10.1016/j.cmpb.2016.03.019.

[46] B.R. Thompson, T.S. Horozov, S.D. Stoyanov, V.N. Paunov, An ultra melt-resistant hydrogel from food grade carbohydrates, RSC Adv. 7 (72) (2017) 45535–45544, http://dx.doi.org/10.1039/C7RA08590G.

[47] M. Watase, K. Arakawa, Rheological properties of hydrogels of agar-agar, Nippon Kagaku Zassi 92 (1) (1971) 37–42, http://dx.doi.org/10.1246/nikkashi1948.92.37, URL http://joi.jlc.jst.go.jp/JST.Journalarchive/nikkashi1948/92.37?from=CrossRef.

[48] G.S. Cowley, B.A. Weir, F. Vazquez, P. Tamayo, J.A. Scott, S. Rusin, A. East-Seletsky, L.D. Ali, W.F. Gerath, S.E. Pantel, P.H. Lizotte, G. Jiang, J. Hsiao, A. Tsherniak, E. Dwinell, S. Aoyama, M. Okamoto, W. Harrington, E. Gelfand, T.M. Green, M.J. Tomko, S. Gopal, T.C. Wong, H. Li, S. Howell, N. Stransky, T. Liefeld, D. Jang, J. Bistline, B. Hill Meyers, S.A. Armstrong, K.C. Anderson, K. Stegmaier, M. Reich, D. Pellman, J.S. Boehm, J.P. Mesirov, T.R. Golub, D.E. Root, W.C. Hahn, Parallel genome-scale loss of function screens in 216 cancer cell lines for the identification of context-specific genetic dependencies, Sci. Data 1 (1) (2014) 140035, http://dx.doi.org/10.1038/sdata.2014.35.

[49] A. Hamburger, S.E. Salmon, Primary bioassay of human myeloma stem cells, J. Clin. Investig. 60 (4) (1977) 846–854, http://dx.doi.org/10.1172/JCI108839.

[50] A.J. Engler, M.A. Griffin, S. Sen, C.G. Bönnemann, H.L. Sweeney, D.E. Discher, Myotubes differentiate optimally on substrates with tissue-like stiffness, J. Cell Biol. 166 (6) (2004) 877–887, http://dx.doi.org/10.1083/jcb.200405004.

[51] N. Huebsch, P.R. Arany, A.S. Mao, D. Shvartsman, O.A. Ali, S.A. Bencherif, J. Rivera-Feliciano, D.J. Mooney, Harnessing traction-mediated manipulation of the cell/matrix interface to control stem-cell fate, Nature Mater. 9 (6) (2010) 518–526, http://dx.doi.org/10.1038/nmat2732, arXiv:NIHMS150003.

[52] Z. Li, X. Guo, A.F. Palmer, H. Das, J. Guan, High-efficiency matrix modulus-induced cardiac differentiation of human mesenchymal stem cells inside a thermosensitive hydrogel, Acta Biomater. 8 (10) (2012) 3586–3595, http://dx.doi.org/10.1016/j.actbio.2012.06.024.

[53] B. Bhana, R.K. Iyer, W.L.K. Chen, R. Zhao, K.L. Sider, M. Likhitpanichkul, C.A. Simmons, M. Radisic, Influence of substrate stiffness on the phenotype of heart cells, Biotechnol. Bioeng. 105 (6) (2010) 1148–1160, http://dx.doi.org/10.1002/bit.22647.

[54] C.P. Jackman, A.M. Ganapathi, H. Asfour, Y. Qian, B.W. Allen, Y. Li, N. Bursac, Engineered cardiac tissue patch maintains structural and electrical properties after epicardial implantation, Biomaterials 159 (2018) 48–58, http://dx.doi.org/10.1016/j.biomaterials.2018.01.002.

[55] Q.Q. Wu, Q. Chen, Mechanoregulation of chondrocyte proliferation, maturation, and hypertrophy: Ion-channel dependent transduction of matrix deformation signals, Exp. Cell Res. 256 (2) (2000) 383–391, http://dx.doi.org/10.1006/excr.2000.4847.

[56] S. Elmore, Apoptosis: A review of programmed cell death, Toxicol. Pathol. 35 (4) (2007) 495–516, http://dx.doi.org/10.1080/01926230701320337, arXiv:NIHMS150003.

[57] E.M. Kearney, P.J. Prendergast, V.a. Campbell, Mechanisms of strain-mediated mesenchymal stem cell apoptosis, J. Biomech. Eng. 130 (6) (2008) 061004, http://dx.doi.org/10.1115/1.2979870.

[58] G. Cheng, J. Tse, R.K. Jain, L.L. Munn, Micro-environmental mechanical stress controls tumor spheroid size and morphology by suppressing proliferation and inducing apoptosis in cancer cells, in: M.V. Blagosklonny (Ed.), PLoS One 4 (2) (2009) e4632, http://dx.doi.org/10.1371/journal.pone.0004632.

[59] P. Urdeitx, S. Clara-Trujillo, J.L.G. Ribelles, M.H. Doweidar, Computational modeling of multiple myeloma growth and tumor aggregate formation, Comput. Methods Progr. Biomed. Update (2022) 100073, http://dx.doi.org/10.1016/j.cmpbup.2022.100073.

[60] E. Menu, R. Kooijman, E.V. Valckenborgh, K. Asosingh, M. Bakkus, B.V. Camp, K. Vanderkerken, Specific roles for the PI3k and the MEK–ERK pathway in IGF-1-stimulated chemotaxis, VEGF secretion and proliferation of multiple myeloma cells: study in the 5T33MM model, Br. J. Cancer 90 (5) (2004) 1076–1083, http://dx.doi.org/10.1038/sj.bjc.6601613.

[61] M.L. Rodriguez, P.J. McGarry, N.J. Sniadecki, Review on cell mechanics: Experimental and modeling approaches, Appl. Mech. Rev. 65 (6) (2013) http://dx.doi.org/10.1115/1.4025355.

[62] J. Ge, L. Guo, S. Wang, Y. Zhang, T. Cai, R.C.H. Zhao, Y. Wu, The size of mesenchymal stem cells is a significant cause of vascular obstructions and stroke, Stem Cell Rev. Rep. 10 (2) (2014) 295–303, http://dx.doi.org/10.1007/s12015-013-9492-x.

[63] T.E.G. Krueger, D.L.J. Thorek, S.R. Denmeade, J.T. Isaacs, W.N. Brennen, Concise review: Mesenchymal stem cell-based drug delivery: The good, the bad, the ugly, and the promise, Stem Cells Transl. Med. 7 (9) (2018) 651–663, http://dx.doi.org/10.1002/sctm.18-0024.

[64] T. Pick, A. Beck, I. Gamayun, Y. Schwarz, C. Schirra, M. Jung, E. Krause, B.A. Niemeyer, R. Zimmermann, S. Lang, E. van Anken, A. Cavalié, Remodelling of Ca2+ homeostasis is linked to enlarged endoplasmic reticulum in secretory cells, Cell Calcium 99 (2021) 102473, http://dx.doi.org/10.1016/j.ceca.2021.102473.

[65] M. Aragona, T. Panciera, A. Manfrin, S. Giulitti, F. Michielin, N. Elvassore, S. Dupont, S. Piccolo, A mechanical checkpoint controls multicellular growth through YAP/TAZ regulation by actin-processing factors, Cell 154 (5) (2013) 1047–1059, http://dx.doi.org/10.1016/j.cell.2013.07.042.

[66] R. Foty, A simple hanging drop cell culture protocol for generation of 3D spheroids, J. Vis. Exp. 51 (51) (2011) http://dx.doi.org/10.3791/2720.

[67] Y. Zhou, S. Uddin, T. Zimmerman, J.-A. Kang, J. Ulaszek, A. Wickrema, Growth control of multiple myeloma cells through inhibition of glycogen synthase kinase-3, Leuk. Lymphoma 49 (10) (2008) 1945–1953, http://dx.doi.org/10.1080/10428190802304966.

[68] A.I. McClatchey, A.S. Yap, Contact inhibition (of proliferation) redux, Curr. Opin. Cell Biol. 24 (5) (2012) 685–694, http://dx.doi.org/10.1016/j.ceb.2012.06.009.

[69] K. Podar, Y.-T. Tai, F.E. Davies, S. Lentzsch, M. Sattler, T. Hideshima, B.K. Lin, D. Gupta, Y. Shima, D. Chauhan, C. Mitsiades, N. Raje, P. Richardson, K.C. Anderson, Vascular endothelial growth factor triggers signaling cascades mediating multiple myeloma cell growth and migration, Blood 98 (2) (2001) 428–435, http://dx.doi.org/10.1182/blood.V98.2.428.

[70] D. Saforo, L. Omer, A. Smolenkov, A. Barve, L. Casson, N. Boyd, G. Clark, L. Siskind, L. Beverly, Primary lung cancer samples cultured under microenvironment-mimetic conditions enrich for mesenchymal stem-like cells that promote metastasis, Sci. Rep. 9 (1) (2019) 4177, http://dx.doi.org/10.1038/s41598-019-40519-4.

[71] J. Barbazan, C. Pérez-González, M. Gómez-González, M. Dedenon, S. Richon, E. Latorre, M. Serra, P. Mariani, S. Descroix, P. Sens, X. Trepat, D. Matic Vignjevic, Cancer-associated fibroblasts actively compress cancer cells and modulate mechanotransduction, BioRxiv (2021) http://dx.doi.org/10.1101/2021.04.05.438443, 2021.04.05.438443.

[72] D.V.F. Tauriello, E. Sancho, E. Batlle, Overcoming TGFβ-mediated immune evasion in cancer, Nat. Rev. Cancer (2021) 1–20, http://dx.doi.org/10.1038/s41568-021-00413-6.

[73] D. Gao, L.T. Vahdat, S. Wong, J.C. Chang, V. Mittal, Microenvironmental regulation of Epithelial–Mesenchymal transitions in cancer, Cancer Res. 72 (19) (2012) 4883–4889, http://dx.doi.org/10.1158/0008-5472.CAN-12-1223.

[74] M.-L. Wang, C.-M. Pan, S.-H. Chiou, W.-H. Chen, H.-Y. Chang, O.K.-S. Lee, H.-S. Hsu, C.-W. Wu, Oncostatin m modulates the mesenchymal–epithelial transition of lung adenocarcinoma cells by a mesenchymal stem cell-mediated paracrine effect, Cancer Res. 72 (22) (2012) 6051–6064, http://dx.doi.org/10.1158/0008-5472.CAN-12-1568.

[75] R. Liu, S. Wei, J. Chen, S. Xu, Mesenchymal stem cells in lung cancer tumor microenvironment: their biological properties, influence on tumor growth and therapeutic implications, Cancer Lett. 353 (2) (2014) 145–152, http://dx.doi.org/10.1016/j.canlet.2014.07.047.

[76] J. Jin, T. Wang, Y. Wang, S. Chen, Z. Li, X. Li, J. Zhang, J. Wang, SRC3 expressed in BMSCs promotes growth and migration of multiple myeloma cells by regulating the expression of Cx43, Int. J. Oncol. 51 (6) (2017) 1694–1704, http://dx.doi.org/10.3892/ijo.2017.4171.

[77] S. Clara-Trujillo, L. Tolosa, L. Cordón, A. Sempere, G.G. Ferrer, J. Luis, G. Ribelles, J.L.G. Ribelles, Novel microgel culture system as semi-solid three-dimensional in vitro model for the study of multiple myeloma proliferation and drug resistance, Biomater. Adv. (2022) 212749, http://dx.doi.org/10.1016/j.bioadv.2022.212749.